

# Correlated $N$ -boson systems for arbitrary scattering length

O. Sørensen, D. V. Fedorov, and A. S. Jensen

*Department of Physics and Astronomy, University of Aarhus, DK-8000 Aarhus C, Denmark*

(Dated: May 22, 2019)

We investigate systems of identical bosons with the focus on two-body correlations and attractive finite-range potentials. We use a hyperspherical adiabatic method and apply a Faddeev type of decomposition of the wave function. We discuss the structure of a condensate as function of particle number and scattering length. We establish universal scaling relations for the critical effective radial potentials. We investigate various decay rates limiting the stability of condensates.

PACS numbers: 31.15.Ja, 05.30.Jp, 21.65.+f

## I. INTRODUCTION

Condensation of a macroscopic number of bosons in the same quantum state was predicted many years ago [1]. Much later this was experimentally achieved in the laboratory for dilute systems of alkali gases [2–4]. The average properties of these gases are accounted for by the Gross-Pitaevskii equation [5, 6]. Exhaustive reviews of the theoretical developments after the experimental breakthrough can be found in [7, 8].

Degrees of freedom beyond the mean-field are crucial for the stability of the condensates, e.g., recombination into bound dimer and trimer cluster states [9–11]. The importance of such correlations is revealed in recent experiments [12, 13]. One example is the collapse of a bose gas with large scattering length [13] where the lack of atoms in the condensate challenged the mean-field description in terms of the time-dependent Gross-Pitaevskii equation [14, 15].

The mean-field description is valid for  $n|a_s|^3 \ll 1$ , where  $n$  is the density and  $a_s$  is the two-body s-wave scattering length, when the particles on average are outside the interaction volume of the order of scattering length,  $a_s$ , to the third power [8]. The mean-field method neglects all correlations and thus breaks down at larger densities where correlations become important. Going beyond the mean-field is often very complicated as exemplified by Jastrow theory [16–18], which leads to high-dimensional equations. A later formulation is contained in the Faddeev-Yakubovskii equations [19, 20] where the wave function is expressed in terms of components describing the asymptotic behaviour of all kinds of clusters.

Comparison of different models is not always straightforward, since different degrees of freedom are treated and the two-body interactions must be renormalized accordingly. For example, using realistic potentials in self-consistent mean-field calculations leads to disastrous results because the Hilbert space does not include correlations [21] as needed to describe both the short- and long-range asymptotic behaviour. In Gross-Pitaevskii calculations the  $\delta$ -function interaction is renormalized to give the correct scattering length in the Born approximation [8]. However, this substitution is only valid in the low-density limit. When correlations are included a different,

and more realistic, interaction must also be used. Furthermore, only average properties can be described in the mean-field approximation. Thus comparisons of correlation dependent quantities are meaningless.

Five years ago an interesting alternative study of a condensate was formulated in terms of hyperspherical coordinates without any two-body correlations [22]. Using the same coordinate system a theoretical frame for describing correlations was given soon after [23]. Detailed three-body calculations with zero total angular momentum were recently performed in the same framework [24]. Here the scattering length is varied and excited three-body states and any number of bound two-body molecular states are allowed. The claim in [24] is that higher-lying Bose-Einstein condensed states in a trap of length  $b_t$  do not collapse when  $N|a_s|/b_t \gtrsim 0.5$  as otherwise indicated by experiments [13]. The recombination takes place at distances several times the scattering length. They conjecture that the properties for  $N > 3$  are quantitatively similar to these three-body results. Another study in the same framework investigates the model-dependence of the three-body energy and finds that only the large scattering length enter [25]. They also indicate that the energy is insensitive to possible higher-order correlations for systems with many particles in a trap.

In a further development using the adiabatic hyperspherical expansion we formulated a method to describe two-body correlations in many-boson systems [26, 27]. This method is a novel attempt to describe correlated systems of low density. The formulation heavily relies on an additive set of components of the wave function as in the Faddeev decomposition but in contrast to the Jastrow multiplicative formulation. The numerical studies were limited to Bose-Einstein condensation for 20 particles.

The purpose of the present paper is to extend the applications to arbitrary scattering lengths and large particle numbers. We want to extract the general properties of the solutions especially for large scattering lengths where mean-field computations are invalid. We obtain naturally self-bound many-body systems, even when the two- and three-body subsystems are unbound. Finally we want to discuss stability criteria for condensates expressed in terms of various time scales and decay rates. In section II we briefly describe the method. In sections III and IV we discuss crucial angular eigenvalues and the radial so-

lutions, respectively. Section V is concerned with decay rates and section VI contains the conclusions.

## II. HYPERSPHERICAL ADIABATIC METHOD

We use the hyperspherical adiabatic expansion method with finite-range two-body interactions and simplifying assumptions about the wave function. We shall briefly describe the method and the assumptions. Details are given in [27].

The system of  $N$  identical particles of mass  $m$  is in the center of mass frame described by hyperspherical coordinates, i.e., one length, the hyperradius  $\rho$ , given by

$$\rho^2 = \frac{1}{N} \sum_{i<j}^N r_{ij}^2 = \sum_{i=1}^N r_i^2 - NR^2 \quad (1)$$

and  $3N-4$  hyperangles  $\Omega$  [23, 28]. The  $i$ th single-particle coordinate is  $\vec{r}_i$ ,  $\vec{R}$  is the center of mass coordinate, and

$$r_{ij} = |\vec{r}_j - \vec{r}_i| \equiv \sqrt{2}\rho \sin \alpha_{ij}, \quad (2)$$

with  $\alpha_{ij} \in [0, \pi/2]$ . The atoms are trapped in an external field approximated by a spherically symmetric harmonic oscillator potential of angular frequency  $\omega$ :

$$V_{\text{ext}} = \sum_{i=1}^N \frac{1}{2} m \omega^2 r_i^2 = \frac{1}{2} m \omega^2 (\rho^2 + NR^2). \quad (3)$$

Without any two-body interaction between the particles the ground-state wave function is a Hartree product of Gaussian amplitudes:

$$\Psi_{\text{total}} = \prod_{i=1}^N e^{-r_i^2/(2b_t^2)} = e^{-\rho^2/(2b_t^2)} e^{-NR^2/(2b_t^2)}, \quad (4)$$

where the trap length is  $b_t = \sqrt{\hbar/(m\omega)}$ . The second radial moments are  $\langle r_i^2 \rangle = 3b_t^2/2$  and  $\langle R^2 \rangle = 3b_t^2/(2N)$ . For large  $N$  the average hyperradius therefore approaches the average mean-field radial coordinate times  $\sqrt{N}$ , see eq. (1). The hyperangles determine the relative orientations of the particles.

With a two-body interaction term  $V(r_{ij})$  the total hamiltonian becomes

$$\hat{H} = \sum_{i=1}^N \left( \frac{\hat{p}_i^2}{2m} + \frac{1}{2} m \omega^2 r_i^2 \right) + \sum_{i<j}^N V(r_{ij}). \quad (5)$$

It separates into a center of mass part ( $\hat{H}_{\text{c.m.}}$ ), a radial part ( $\hat{H}_\rho$ ), and an angular part ( $\hat{h}_\Omega$ ) depending respec-

tively on  $\vec{R}$ ,  $\rho$ , and  $\Omega$  [28]:

$$\hat{H} = \hat{H}_{\text{c.m.}} + \hat{H}_\rho + \frac{\hbar^2 \hat{h}_\Omega}{2m\rho^2}, \quad (6)$$

$$\hat{H}_{\text{c.m.}} = \frac{\hat{p}_R^2}{2Nm} + \frac{1}{2} Nm\omega^2 R^2, \quad (7)$$

$$\hat{H}_\rho = \hat{T}_\rho + \frac{1}{2} m\omega^2 \rho^2, \quad (8)$$

$$\frac{\hbar^2 \hat{h}_\Omega}{2m\rho^2} = \hat{T}_\Omega + \sum_{i<j} V_{ij}, \quad (9)$$

where  $\hat{T}_\rho$  and  $\hat{T}_\Omega$  are radial and angular kinetic energy operators. Then the center of mass motion always separates from the relative motion since the  $V_{ij}$ -terms are independent of  $R$ .

We remove the center of mass motion and study the Schrödinger equation for relative coordinates

$$(\hat{H} - \hat{H}_{\text{c.m.}})\Psi = E\Psi. \quad (10)$$

The adiabatic hyperspherical expansion of the wave function is

$$\Psi(\rho, \Omega) = \rho^{-(3N-4)/2} \sum_{\nu=0}^{\infty} f_\nu(\rho) \Phi_\nu(\rho, \Omega), \quad (11)$$

where  $\Phi_\nu$  is an eigenfunction of the angular part of the hamiltonian with an eigenvalue  $\hbar^2 \lambda_\nu(\rho)/(2m\rho^2)$ :

$$\hat{h}_\Omega \Phi_\nu(\rho, \Omega) = \lambda_\nu(\rho) \Phi_\nu(\rho, \Omega). \quad (12)$$

Then eq. (10) leads to a set of coupled radial equations. Neglecting couplings between the different  $\nu$ -channels yields the radial eigenvalue equation:

$$\left( -\frac{\hbar^2}{2m} \frac{d^2}{d\rho^2} + U_\nu(\rho) - E_\nu \right) f_\nu(\rho) = 0, \quad (13)$$

$$\frac{2mU_\nu(\rho)}{\hbar^2} = \frac{\lambda_\nu}{\rho^2} + \frac{(3N-4)(3N-6)}{4\rho^2} + \frac{\rho^2}{b_t^4}, \quad (14)$$

where  $E_\nu$  is the energy and the adiabatic potential  $U_\nu$  acts as an effective mean-field potential as a function of the hyperradius. This potential consists of three terms, i.e., the external field, the generalized centrifugal barrier, and the angular average of the interactions and kinetic energies. The neglected non-diagonal terms are typically about 1% of the diagonal terms for attractive Gaussian potentials.

We have so far no restriction on the many-body wave function, but include in principle any structure of the system. To choose a convenient form we follow the philosophy in the Faddeev-Yakubovskii formulations [19, 20], i.e., the additive decomposition of the wave function reflects explicitly the possible asymptotic large-distance behaviour of cluster subsystems. We expect that two-body correlations are most important and we select the corresponding terms in the decomposition. Higher-order

correlations are then essentially neglected. This procedure assumes a very different starting point compared to the Jastrow factorization into products of two-body wave functions [16, 29, 30]. The traditional Jastrow form is expected to be more efficient for large densities while our method is well suited for the low densities encountered for Bose-Einstein condensates.

Emphasizing two-body correlations we therefore decompose the angular wave function  $\Phi$  in the symmetric Faddeev components  $\phi$

$$\Phi(\rho, \Omega) = \sum_{i<j}^N \phi_{ij}(\rho, \Omega) \approx \sum_{i<j}^N \phi(\rho, r_{ij}) , \quad (15)$$

where the last approximation assumes that only relative s-waves between each pair of particles contribute. Then the coordinate dependence reduces to the distance  $r_{ij} = \sqrt{2}\rho \sin \alpha_{ij}$ . Neglecting higher-order partial waves is justified when the large-distance properties are decisive. The capability of this assumption for large scattering length has been demonstrated for  $N = 3$  by describing the intricate Efimov effect [31, 32].

The angular eigenvalue equation, eq. (12), can by a variational technique be rewritten as a second order integro-differential equation in the variable  $\alpha_{12}$  [28]. For atomic condensates the interaction range is very short compared to the spatial extension of the  $N$ -body system. Then this equation simplifies even further to contain at most one-dimensional integrals. The validity of our approximations only relies on the small *range* of the potential, whereas the scattering length can be as large as desired.

We shall use the finite-range Gaussian potential  $V(r) = V_0 \exp(-r^2/b^2)$  and study the dependence on the scattering length  $a_s$ . It is convenient to measure the strength of the interaction in units of the Born-approximation of the scattering length

$$a_B \equiv \frac{m}{4\pi\hbar^2} \int d^3\vec{r}_{kl} V(\vec{r}_{kl}) = \frac{\sqrt{\pi}mb^3V_0}{4\hbar^2} , \quad (16)$$

where the last expression is for the Gaussian potential. We use the sign convention that  $a_s > 0$  for a purely repulsive potential, such that  $a_s \simeq a_B$  for  $|a_B|/b \ll 1$ . In appendix A is collected the connections between the Gaussian strength measured in  $a_B/b$  and the scattering length  $a_s/b$  for the cases applied in this work. In most of the numerical work we have  $|a_B|/b$  close to unity.

### III. ANGULAR POTENTIALS

The key quantity in the radial equation of motion is the angular eigenvalue  $\lambda$  obtained from eq. (12). This eigenvalue depends on the number of particles, on the size of the system through the hyperradius, and on the potential through the scattering length. The behaviour

of  $\lambda$  is decisive for the effective potential which in turn determines the properties of the solutions. We shall therefore first study the dependence of  $\lambda$  on the parameters in the model. We use the method described in [27]. The two-body interaction is in mean-field computations often assumed to be repulsive to avoid the collapse at short distance arising from the  $\delta$ -force [33]. This problem is not present for finite-range interactions, and we can as well use attractive potentials.

#### A. General eigenvalue behaviour

The angular eigenvalue spectrum coincides with the free spectrum (without interaction) at both small and large hyperradii; for  $\rho = 0$  because all interactions are multiplied by  $\rho^2$  and at  $\rho = \infty$  because the short-range interaction has no effect at large distances. Thus, perturbation theory for a Gaussian potential shows that for small  $\rho$  the eigenvalues all change from their hyperspherical values  $\lambda_\nu(0) = 2\nu(2\nu + 3N - 5)$ ,  $\nu = 0, 1, \dots$ , as

$$\lambda_\nu(\rho) - \lambda_\nu(0) = \frac{mV_0}{\hbar^2} N(N-1)\rho^2 . \quad (17)$$

If the two-body potential is attractive, but too weak to support any bound state, the eigenvalues reach a minimum and then return to one of the finite hyperspherical values. For any two-body bound state of energy  $E^{(2)}$  one eigenvalue diverges as  $\lambda = 2mE^{(2)}\rho^2/\hbar^2$ . The corresponding structure describes, appropriately symmetrized, one pair of particles in that bound state and all others far apart from the pair and from each other. In addition to this finite number of such eigenvalues the hyperspherical spectrum emerges at large distances.

To illustrate we show in fig. 1 a number of possible angular eigenvalues  $\lambda$  as functions of hyperradius for different potentials. The entirely positive (solid) curve corresponds to a repulsive Gaussian. The diverging (dotted and thick dot-dashed) curves correspond to potentials with one bound two-body state. For our purpose the curves approaching zero for large  $\rho$  (dashed and thin dot-dashed curves) are the most interesting, since they are crucial for the description of the condensate. This is true even in the presence of lower-lying states (dot-dashed curve) which are essential doorway states for decay of the condensate.

The convergence of  $\lambda$  as  $\rho \rightarrow 0$  is due to the finite range of the potential and depends on the interaction range  $b$ . The deep minima at small to intermediate distances depend strongly on both the number of particles and the strength of the attraction. They are substantially deeper than reported in [26, 27] where one term inadvertently was used with the wrong sign in the numerical examples. Increasing the strength of the attraction leads to larger negative values of  $\lambda$ . This trend continues by increasing the attraction even further until the same scattering length is reached but now with one bound two-body state.

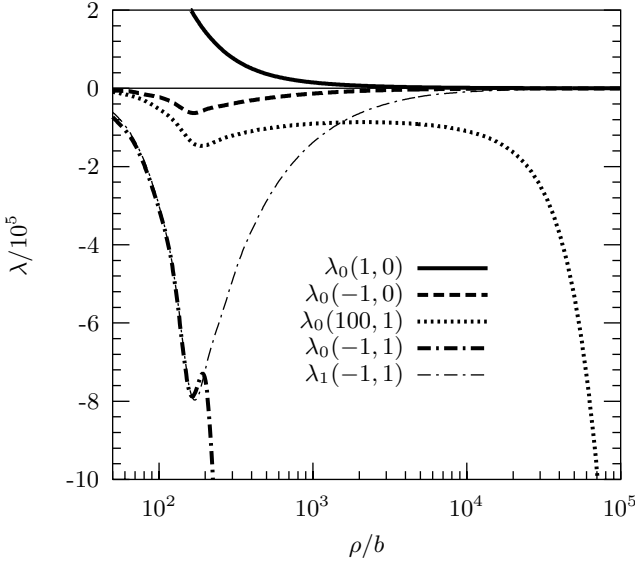


FIG. 1: Angular eigenvalues  $\lambda_\nu$  (divided by  $10^5$ ) as functions of hyperradius divided by interaction range,  $\rho/b$ , for  $N = 100$ , for scattering lengths  $a_s/b$  and numbers of bound two-body states  $\mathcal{N}_B$  indicated as  $\lambda_\nu(a_s/b, \mathcal{N}_B)$  on the figure.

For distances much larger than the range of the potential the eigenvalues could as well be computed from a zero-range interaction, i.e.,  $4\pi\hbar^2 a_s \delta(\vec{r})/m$ . The hyperharmonic angular wave function should then be appropriate for  $\Phi$  and the eigenvalue  $\lambda$  obtained as the corresponding expectation value. The lowest hyperharmonic is a constant independent of angles and the result is [22]

$$\begin{aligned} \lambda_\delta(N, \rho) &= \sqrt{\frac{2}{\pi}} \frac{\Gamma(\frac{3N-3}{2})}{\Gamma(\frac{3N-6}{2})} N(N-1) \frac{a_s}{\rho} \\ &\xrightarrow{N \gg 1} \frac{3}{2} \sqrt{\frac{3}{\pi}} N^{7/2} \frac{a_s}{\rho}. \end{aligned} \quad (18)$$

This zero-range result is inversely proportional to  $\rho$  for all hyperradii and consequently with a non-physical divergence when  $\rho \rightarrow 0$ . The only length scale arises from the strength of the  $\delta$ -function. In mean-field calculations this strength is chosen to reproduce the correct scattering length  $a_B$  in the Born approximation [8, 21]. To reach this limit with a Gaussian potential then requires that the  $\delta$ -function is approached while  $a_B$  is maintained equal to the desired value of  $a_s$ .

This artificial construction is due to the lack of correlations in mean-field computations where the effective interaction is adjusted to the available Hilbert space. We use finite-range Gaussian potentials and include two-body correlations. Then we expect the large-distance asymptotic behaviour to reveal the correct scattering length as in eq. (18) without any renormalization of the interaction potential. This tests the efficiency of the simplified structure of the wave function in eq. (15). Mathematically this should result from the structure of the

second order integro-differential angular eigenvalue equation [27, 28].

Numerically we investigate the asymptotic behaviour of  $\lambda$  in this context by comparing to the zero-range result  $\lambda_\delta$  in fig. 2. The convergence to the limiting value is fastest for the smallest value of  $a_s$  (dashed curve) already reflecting that the correlations arising for large scattering lengths (dotted line) cannot be accounted for by the simple zero-range result. This is well understood for three particles where the Efimov effect (very large  $a_s$ ) extends correlations in hyperradius to distances around four times the average scattering length [31, 32]. These effects are not present in the mean-field type of zero-range expectation value contained in  $\lambda_\delta$ . When  $\rho$  exceeds  $a_s$  by a sufficiently large amount the Efimov effect can no longer be seen in  $\lambda$  and  $\lambda_\delta$  is approached.

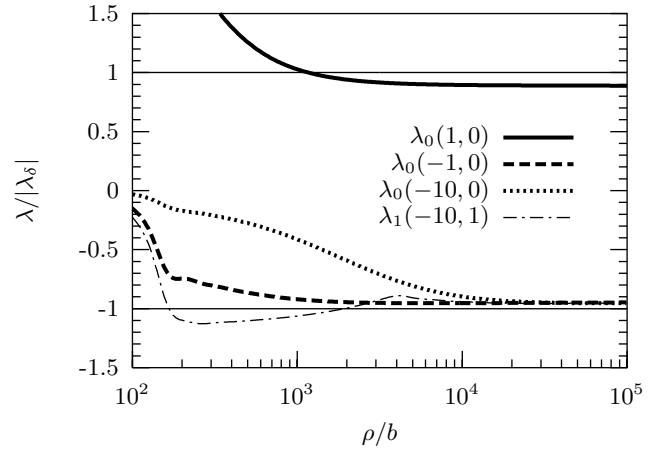


FIG. 2: Same as figure 1, but the angular potential is shown in units of the zero-range result in eq. (18).

The positive scattering length also leads to an eigenvalue approaching  $\lambda_\delta$  at large distance, now seen as a convergence towards  $+1$  with a similar convergence rate (solid curve). A stronger attraction corresponding to one bound two-body state produces one diverging eigenvalue while the second eigenvalue converges towards the lowest hyperspherical value (dot-dashed curve). In fact it almost coincides with the lowest eigenvalue for the same scattering length but for a potential without bound two-body states (dotted curve).

The deviations from  $\lambda_\delta$  at large distance is in all cases less than 10%. The asymptotic behaviour is very smooth but still originating in systematic numerical inaccuracies which can be cured by increasing the number of integration points. However, this requires a major effort if it has to be done in all computations. Instead we exploit our mathematical knowledge about the asymptotic behaviour and thereby avoid the numerical problems while increasing the accuracy.

These numerical results show the potential-independence of the large-distance properties when

$a_s$  remains finite, i.e., the scattering length determines entirely the asymptotic behaviour, and the details of the potentials are unimportant. The radial shape of the two-body potential could be Gaussian, square-well, Woods-Saxon, or Yukawa, still the same  $a_s$  would produce the same angular eigenvalue at sufficiently large distance.

### B. $N$ -dependence

The angular eigenvalues increase rapidly with  $N$  as seen already from the  $N^{7/2}$ -dependence in  $\lambda_\delta$ . The major variation in magnitude is then accounted for by using this large-distance zero-range result as the scaling unit. We show in fig. 3 a series of calculations for the same two-body interaction for different numbers of atoms. All curves are similar with a systematic increase in the characteristic hyperradius where they bend and approach the zero-range result. We know that the large-distance asymptotics is determined by the scattering length. We can then define the characteristic length  $\rho_a$  by

$$\rho_a(N) \equiv |a_s|N^{7/6}, \quad (19)$$

where the particular power of  $7/6$  is found numerically.

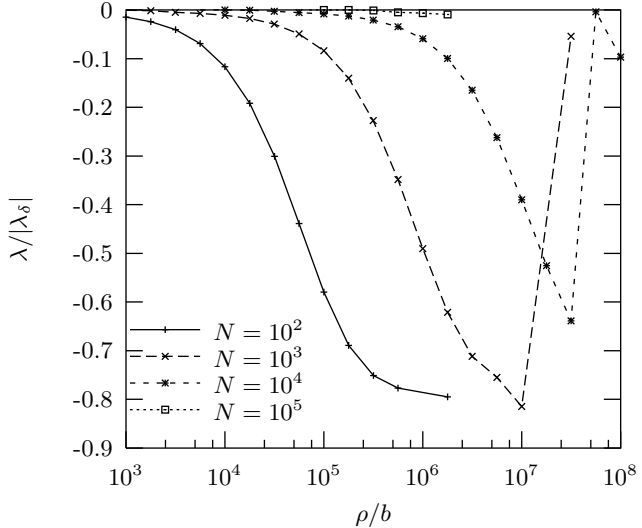


FIG. 3: The lowest angular eigenvalue as a function of hyperradius for  $a_s/b = -401$  for four different numbers of particles  $N = 10^2, 10^3, 10^4, 10^5$ . The angular potentials are in units of  $|\lambda_\delta|$ .

The quality of this scaling is seen in fig. 4, where all curves essentially coincide for distances smaller than  $\rho_a$ . At larger hyperradii the zero-range result of  $-1$  should be obtained. However, here numerical inaccuracies produce systematic deviations from a common curve, i.e., the deviations increase with  $N$ . Furthermore for each  $N$  one smooth curve is followed at small and intermediate distances implying that the inaccuracies here are systematic until at some point random fluctuations sets

in. This observation can be exploited to improve the numerical procedure but it also allows extraction of more accurate results without increasing the already substantial numerical efforts.

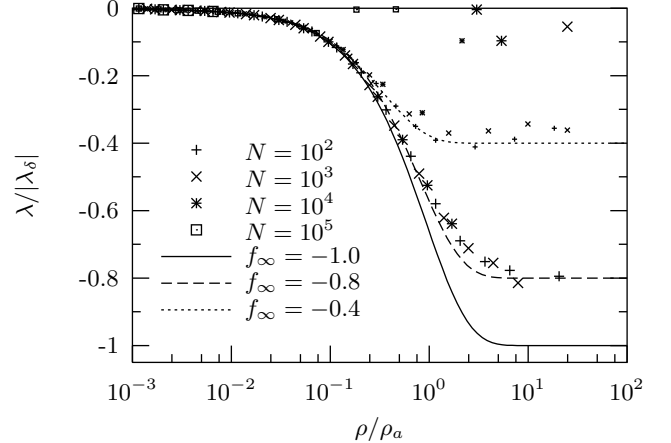


FIG. 4: The same as fig. 3, but with  $\rho$  in units of  $\rho_a$ . The larger points following the intermediate curve ( $g_\infty = -0.8$ ) are calculated with the highest numerical accuracy and the smaller points along the upper curve ( $g_\infty = -0.4$ ) are obtained with lower accuracy. The curve for  $g_\infty = -1.0$  is the expected correct asymptotic behaviour.

The smooth numerical curves can be rather well reproduced by the function

$$\lambda^{(-)}(N, \rho) = |\lambda_\delta(N, \rho)| \cdot g^{(-)}(\rho/\rho_a), \quad (20)$$

$$g^{(-)}(x) = g_\infty \left( 1 - e^{-x/x_a} \right) \left( 1 + \frac{x_b}{x} \right), \quad (21)$$

where  $g_\infty$  has the value  $-1$  in accurate calculations, because  $a_s < 0$ . The exponential term is introduced to reproduce the rather steep approach to the asymptotic value as seen in fig. 4. The behaviour at smaller distance, depending on the range of the interaction, is here simulated by the  $x_b$ -term. The extreme limit of  $\rho \rightarrow 0$  is not computed and not included in the approximate function in eq. (21).

The two groups of computations in fig. 4 are reasonably well reproduced by the parameter sets  $x_a \simeq 0.74$ ,  $x_b \simeq 2.3 \cdot 10^{-3}$ , and  $g_\infty \simeq -0.8$  or  $g_\infty \simeq -0.4$  for the high and low accuracy, respectively. These parameters may also depend on the scattering length. We show therefore in table I the best choice of parameters for different  $a_s$ .

We notice that  $-g_\infty$  and  $x_a$  both are of order unity, and that the fraction  $g_\infty/x_a$  is almost constant, except for the smallest scattering length. The parameter  $x_b$ , introduced to account for the finite interaction range, is almost equal to  $b/|a_s|$ .

At large hyperradii, where  $x_a \ll \rho/\rho_a$  or equivalently  $\rho \gg N^{7/6}|a_s|$ ,  $\lambda^{(-)}$  approaches  $g_\infty|\lambda_\delta|$ . As argued before we expect that the large-distance asymptotics is  $\lambda^{(-)} \rightarrow \lambda_\delta$  and  $g_\infty$  must therefore approach  $-1$  in increasingly accurate calculations. The results for  $N = 100$

TABLE I: Numerical values of  $g_\infty$ ,  $x_a$ , and  $x_b$  for four scattering lengths.

$a_s/b$	-5.98	-401	-799	-4212
$-g_\infty$	0.99	0.80	0.65	0.30
$x_a$	1.06	0.74	0.59	0.28
$-g_\infty/x_a$	0.93	1.081	1.099	1.077
$x_b$	0.15	$2.3 \cdot 10^{-3}$	$1.15 \cdot 10^{-3}$	$2.2 \cdot 10^{-4}$
$x_b/(b/ a_s )$	0.92	0.922	0.919	0.927

and different scattering lengths, see fig. 2, confirm this conclusion by deviating less than 10% from  $\lambda_\delta$  at large hyperradii.

We compare with the well established results for  $N = 3$  where three identical bosons lead to the large-distance behaviour [32]

$$\lambda_\delta(N = 3, \rho) = \frac{48a_s}{\sqrt{2}\pi\rho} \quad (22)$$

in agreement with  $\lambda_\delta$  obtained from eq. (18) for  $N = 3$ . Then the universal function  $g^{(-)}$  asymptotically approaches  $g_\infty = -1$  for all scattering lengths.

We have now demonstrated that the function  $g^{(-)}$  to a good approximation is independent of  $N$ . This combined with the conclusion for  $N = 3$  implies that  $g_\infty = -1$  is valid for all scattering lengths and particle numbers.

The angular eigenvalue is given by  $g^{(-)}(x) \simeq g_\infty x/x_a$  for  $x_b \ll \rho/\rho_a \ll x_a$ . Numerical calculations in this intermediate region of hyperradii therefore rather accurately determines the fraction  $g_\infty/x_a \simeq -1.08$  as given in table I. With  $g_\infty = -1$  this implies that  $x_a \simeq 1/1.08 \simeq 0.92$ . The parameters of  $g^{(-)}(x)$  in eq. (21) can now be collected to be

$$g_\infty = -1, \quad x_a \simeq 0.92, \quad x_b \simeq 0.92 \frac{b}{|a_s|}. \quad (23)$$

The accuracy of the parametrization is seen in figs. 5a-d, where the angular eigenvalues are shown in units of  $\lambda^{(-)}$  with the individual set of parameters from table I. A fairly good agreement is found for  $\rho/\rho_a > x_b$ . The remaining deviations occur at small hyperradii, which is not included in the  $g^{(-)}$ -parametrization, and at large hyperradii where the numerical inaccuracy increases with increasing scattering lengths. On the other hand the large-distance behaviour is known from analytic considerations and we do not need to rely on numerical computations at these distances.

### C. $N$ -dependence with bound two-body states

In the presence of a bound two-body state of identical bosons of masses  $m$  one angular eigenvalue eventually diverges at large hyperradii as

$$\lambda^{(2)}(\rho) = \frac{2m\rho^2}{\hbar^2} E^{(2)}, \quad E^{(2)} < 0, \quad (24)$$

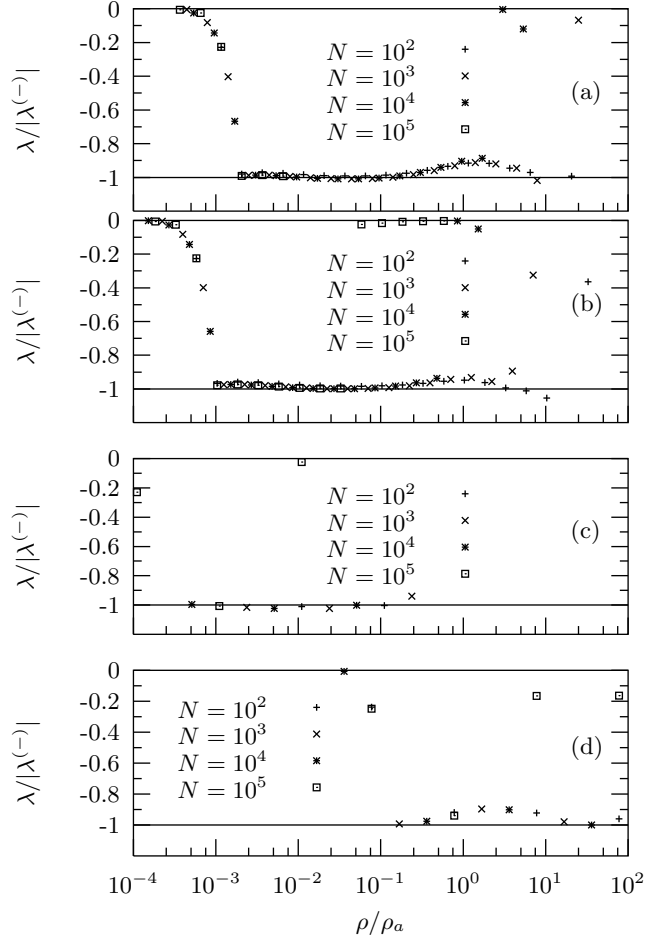


FIG. 5: The lowest angular eigenvalue  $\lambda$  in units of  $\lambda^{(-)}$ , eqs. (20) and (21) and table I, as functions of the hyperradius in units of  $\rho_a$ , eq. (19). The scattering lengths are given by a)  $a_s/b = -401$ , b)  $a_s/b = -799$ , c)  $a_s/b = -4212$ , and d)  $a_s/b = -5.98$ . The different  $N$ -values are as indicated.

where  $E^{(2)}$  is the energy of the two-body bound state. In the limit of weak binding, or in general for numerically large scattering lengths, the energy of the two-body bound or virtual state is given by

$$E^{(2)} = -\frac{\hbar^2}{ma_s^2}c, \quad (25)$$

where  $c$  approaches unity for large scattering lengths.

We now parametrize the angular eigenvalue by an expression similar to eqs. (20) and (21). The effect of the bound two-body state is only expected to show up at large distances where the behaviour corresponds to eq. (25). The small and intermediate distances resemble the behaviour when no bound state is present. Therefore we arrive at the parametrization

$$\lambda^{(+)}(N, \rho) = |\lambda_\delta(N, \rho)| g^{(+)}(\rho/\rho_a), \quad (26)$$

$$g^{(+)}(x) = x \left(1 + \frac{x_b}{x}\right) \left( \frac{g_\infty}{x_a} - c \frac{4}{3} \sqrt{\frac{\pi}{3}} x^2 \right), \quad (27)$$

with the notation and estimates from eq. (23), i.e.,  $x_b \simeq 0.92b/|a_s|$  and  $g_\infty/x_a \simeq -1.08$ . There is no linear term in the second bracket of this expression because we only aimed at the correct behaviour in the limits of small to intermediate and large hyperradii.

We compare in fig. 6 the parametrization in eqs. (26) and (27) with the computed angular eigenvalues for a potential with one bound two-body state. For the large scattering length in fig. 6a one smooth curve applies for all the particle numbers; numerical inaccuracies set in at larger hyperradii, which is most obvious for the largest particle numbers. This smooth curve is in a large interval of hyperradii at most deviating by 20% from the parametrized form, and even less than 10% at large hyperradii, before the numerical instability sets in.

The large-distance deviation is partly due to the diagonal part of the coupling term which is essential to restore the correct asymptotic behaviour [34]. This is also indicated by a calculation for smaller  $a_s$  ( $a_s/b = +10$ ) where the corresponding deviation is less than 1%. The shape at intermediate distances could be improved for example by inclusion of a linear term in eq. (27). The smooth curve at small hyperradii is outside the range of validity of the parametrization, i.e., within the range of the two-body potential and then depending on details of the interaction.

The lowest eigenvalue diverges at large hyperradius as described in connection with fig. 6a and eq. (26). If the two-body potential only has one bound state the second eigenvalue is expected to approach zero at large distances as  $\lambda_\delta$ . This pattern should be repeated with more than one bound two-body state, i.e., the first non-divergent angular eigenvalue should behave as  $\lambda_\delta$  for large  $\rho$ .

We therefore in fig. 6b compare the computed first excited angular eigenvalue with  $\lambda_\delta$  for different  $N$ . As in fig. 4 we obtain smooth and almost universal curves at small  $\rho$ , where the approach to unity sets in exponentially fast depending on  $N$ , but now for  $\rho$  one or two orders of magnitude larger than  $\rho_a$ . Clearly a parametrization would also here be possible.

The large-distance asymptotic behaviour of the first excited state now corresponds to a repulsive potential as seen by the approach to +1. However, at small and intermediate hyperradii the potential is attractive ( $\lambda_1 < 0$ ) which might allow a self-bound system located at distances far inside and independent of the otherwise necessary confining external trap potential.

This feature is absent in the mean-field description of Bose-Einstein condensation. For overall repulsive potentials corresponding to positive scattering lengths no attractive part is possible and for attractive potentials either a zero-range potential would produce a collapsed wave function or a finite-range potential would give converged results but no repulsion at large distance. Mean-field computations usually describe the condensate as the ground state of the many-body system in a confining field.

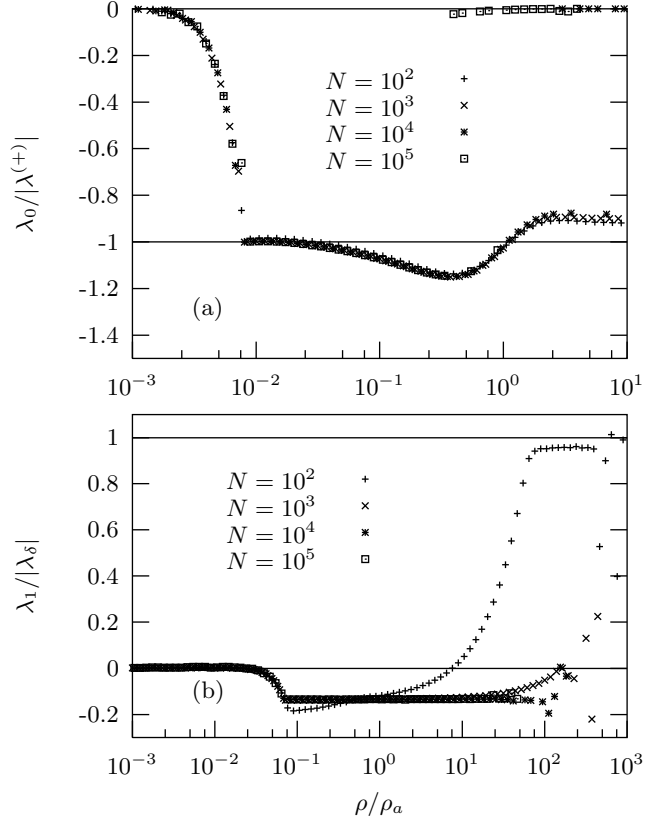


FIG. 6: a) The lowest angular eigenvalue  $\lambda_0$  in units of  $\lambda^{(+)}$ , eqs. (26) and (27), for  $a_s/b = +100$  and  $c = 1.02$ , when the potential holds one bound two-body state. The number of particles is indicated on the figure. The parameters are  $g_\infty/x_a = -1.09$  and  $x_b = 9.2 \cdot 10^{-3}$ . b) The first excited angular eigenvalue  $\lambda_1$  in units of  $\lambda_\delta$  for  $a_s/b = +10$ .

#### D. The properties of $\lambda^{(\pm)}$

The name  $\lambda^{(\pm)}$  indicates the two signs of the scattering length corresponding to bound (+) or unbound (−) two-body systems. Only the behaviour at large hyperradii, when  $\rho > \rho_a$  is different for the two cases. The behaviour at smaller hyperradii is independent of the sign of the scattering length, only the magnitude matters. At small hyperradii when  $\rho/\rho_a < x_b$  the calculations cannot be approximated by  $\lambda^{(\pm)}$ .

At intermediate hyperradii,  $x_b \ll \rho/\rho_a \ll x_a$ , which with  $x_b \sim b/|a_s|$  and  $x_a \sim 1$  becomes

$$b \ll \frac{\rho}{N^{7/6}} \ll |a_s|, \quad (28)$$

the angular eigenvalue is independent of the short-range details of the two-body interaction and the scattering length, so  $\lambda^{(\pm)}$  approaches a constant value. This constant is given by

$$\lambda_\infty \equiv -\lambda_\delta \frac{\rho g_\infty}{\rho_a x_a} = \frac{3g_\infty}{2x_a} N^{7/3} \sqrt{\frac{3}{\pi}} \simeq -1.59 N^{7/3}. \quad (29)$$

This numerical result agrees with a derivation in sim-

ple physical terms in appendix B, which yields  $\lambda_\infty = -1.65N^{7/3}$ . However, the  $N$ -dependence cannot be predicted from the angular equation, since the result is an interplay between the various terms.

The symbol  $\lambda_\infty$  is chosen for this constant, since the relevant  $\rho$ -region extends to infinity for the limit of infinitely large scattering length. With no bound two-body states ( $a_s < 0$ ) the lowest angular eigenvalue approaches zero at larger hyperradii, whereas it diverges towards  $-\infty$  as  $\rho^2$  when a bound two-body state is present ( $a_s > 0$ ). On the threshold for a two-body bound state  $a_s = \pm\infty$  and the angular eigenvalue therefore remains constant. For finite but large  $a_s$  the eigenvalue lingers, cannot decide which way to go, until the hyperradius exceeds a size proportional to the scattering length.

In [26]  $\lambda_\infty \simeq -5N^2$  was estimated by courageous extrapolation of calculations for  $N = 10, 20, 30$  and the analytic result for  $N = 3$ . The much better estimate in eq. (29) of the large- $N$  asymptotics of  $\lambda_\infty(N)$  increases with a slightly higher power of  $N$  but with a smaller proportionality factor.

At large hyperradii,  $\rho \gg \rho_a$ , the behaviour depends on the sign of the scattering length  $a_s$ . When  $a_s < 0$  then  $\lambda^{(\pm)} \simeq \lambda_\delta$ , which is the expectation value of a zero-range interaction for a constant angular wave function eq. (18). This is also equivalent to the mean-field Gross-Pitaevskii result. When  $a_s > 0$  then  $\lambda^{(\pm)} \simeq \lambda^{(2)}$ , which is the signature of a bound two-body state. There is no analogue to this in the mean-field model.

#### IV. RADIAL POTENTIALS AND SOLUTIONS

The radial equation is the next step in the process of obtaining knowledge about the physical properties of the many-boson system. The angular potentials found in the previous section now enter the effective radial potential in eq. (14) and transfer information about the interactions to quantities like energy, size, and structure of the system.

##### A. Properties of the radial potential

The radial potential consists of three terms where the repulsive centrifugal barrier and the confining external field both are positive. The interaction term can be either repulsive or attractive. The combination has structure depending on the interaction. For a purely vanishing or repulsive two-body potential we arrive at a simple behaviour qualitatively similar to the non-interacting (dashed) curve shown in fig. 7 for  $N = 100$ . All solutions are confined to the region between the infinitely large potential walls at small and large hyperradii.

For a moderately attractive potential a different structure already appears in the lowest angular potential (solid curve). The large-distance behaviour is roughly as without interaction, but the barrier at intermediate distance

is now finite both in height and width. The barrier height is small compared to the potential at both small and large hyperradii. At smaller hyperradii a rather deep and relatively narrow minimum is present outside an infinite, repulsive core. The minimum occurs for  $N = 100$  at about 150 times the range of the interaction which corresponds to a mean distance between each pair of particles of about 15 times the interaction range  $b$ .

With this potential the diagonal radial equation is solved. The solutions can be divided into groups related to either the first or the second minimum. The lowest-lying of the first group of solutions have negative energies. They are truly bound states as they cannot decay into continuum states at large hyperradii [26]. Their properties are independent of the external trap which only has an influence at much larger distances. These self-bound  $N$ -body states can decay into lower-lying states consisting of various bound cluster states, e.g., a number of diatomic or triatomic clusters. The possibility of self-bound many-body systems, even though the two- and three-body sub-systems are unbound, is also discussed by Bulgac [35], who, however, considers the three-body interaction strength as a determining parameter for the properties of the self-bound many-boson system.

The group of states in the higher-lying minimum all have positive energies. They are only stable due to the confining effect of the external trap potential. The lowest of these is interpreted as the state of the condensate and indicated by a horizontal line in fig. 7b. The second minimum almost coincides with the minimum of the radial potential arising without any two-body interaction. Thus the structure of the condensate is similar for attractive and repulsive interactions (positive and negative scattering lengths). However, an attraction produces a series of lower-lying states at smaller hyperradii.

Increasing  $N$  leaves semi-quantitatively the same features for pure repulsion. An unchanged attraction leads to decreasing barriers at intermediate hyperradius and at some point this barrier vanishes altogether. At the same time the attractive minimum at smaller hyperradius becomes deeper. This in turn leads to an increasing number of bound states in this minimum as function of  $N$ .

As the scattering length increases, the barrier disappears and the effective potential inside the trap has the  $\rho^{-2}$ -behaviour characteristic for Efimov states. The lowest-lying states are in general influenced by the details of the two-body interaction and without Efimov features. However, the higher-lying states clearly exhibit the Efimov scaling. They quickly become very large and are located far outside the minimum. Only a finite number is possible due to the confining external field.

These states are many-body Efimov states arising when the two-body scattering length is large. This is precisely the condition for the three-body Efimov states [31, 36]. Therefore the many-body Efimov states are embedded in the continua of dimer, trimer and higher-order cluster states. They could be artifacts of the model where only special degrees of freedom are treated. How-

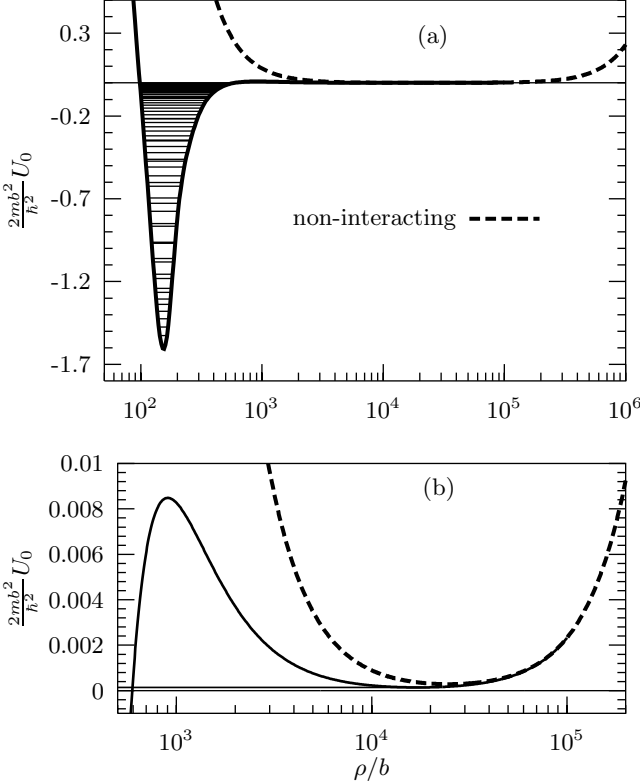


FIG. 7: a) Radial potential  $U_0$  from eq. (14) corresponding to the lowest angular potentials for  $N = 100$  and  $a_s/b = -1.0$ . We model the experimentally studied systems [12] of  $^{85}\text{Rb}$  atoms with oscillator frequency  $\nu = \omega/(2\pi) = 205$  Hz and interaction range  $b = 10$  a.u., thus yielding  $b_t \equiv \sqrt{\hbar/(m\omega)} = 1442b$ . Also shown as horizontal lines are the negative energies  $E_{0,n}$ ,  $n = 0, \dots, 58$  in the lowest potential in the uncoupled radial equation, eq. (13). b) Detail at larger hyperradii. The energy of the first oscillator-like state (see text) is shown as a horizontal line close to zero.

ever, these states may also be distinguishable resonance structures which are relatively stable because the particles are very far from each other and the couplings to the continuum states therefore are very weak. So far this remains an open question.

### B. Definition of a condensate

We focus on the state of the condensate in the second minimum and in the present work only use the lower-lying negative-energy states in connection with the possible decay of the condensate. However, first we want to discuss a definition of a condensate state in the present context.

In mean-field treatments, with repulsive two-body potentials and confining trap potentials, the condensate is uniquely defined as a statistical mixture of single-particle states with the ground state dominating [8, 37]. A con-

densate has on average many particles in the lowest single-particle state. This many-body state is only stable due to the trap and as such first of all determined by the properties of the trap. The many-body state is at best only approximately stationary due to the neglected degrees of freedom which allow energetically favored di- and tri-atomic cluster states. This instability is also an experimental fact seen by permanent loss of trapped atoms, e.g., in recombination processes [13].

Without any two-body interaction the properties of the many-body system is determined by the thick, dashed potential curve in fig. 7. Then we can easily identify the condensate as a state in this potential where the dominating component is the ground state. Including attractive interactions (full curve) the deep minimum at small hyperradius is produced. Then the corresponding ground state, located in this minimum, has nothing to do with a condensate. The density is so high that couplings to other degrees of freedom would develop higher-order correlations and processes like three-body recombinations would quickly destroy the single-atom nature of the gas. This ground state, before or after recombinations, does not show the signature of a Bose-Einstein condensate, where many particles occupy one single-particle level.

The formulation in the present work does not use the concept of single-particle levels. Therefore we cannot talk about a statistical distribution of particles with the majority in the lowest state. However, we can talk about a many-particle system described as a superposition of many-body eigenstates, where the lowest states are favored in thermal equilibrium. To clarify we can think of a quantum state as a superposition of the eigenstates  $\Psi_n(\rho, \Omega)$  in eq. (11) given by

$$\begin{aligned} \Psi_{\text{quantum state}}(\rho, \Omega) &= \sum_{n=0}^{\infty} c_n \Psi_n(\rho, \Omega) \\ &= \rho^{-(3N-4)/2} \sum_{n=0}^{\infty} c_n \sum_{\nu=0}^{\infty} f_{\nu,n}(\rho) \Phi_{\nu}(\rho, \Omega), \end{aligned} \quad (30)$$

with the normalization  $\sum_n |c_n|^2 = 1$ . A condensate must be sufficiently large to exceed a certain minimum interparticle distance,  $d_c$ , below which the atoms are too close and recombine very fast. This distance depends on the scattering length and on the number of particles. Therefore, in our formulation the stationary states cannot be characterized as a condensate if components with  $\langle r_{ij}^2 \rangle \ll d_c^2$  are dominating contributions in the wave function  $\Psi_n(\rho, \Omega)$ .

We define one of the stationary states in this model as the “ideal condensate” state, i.e., the state of lowest energy with one component, labeled by the quantum numbers  $\nu_c$  and  $n_c$ , which has

$$\langle r_{ij}^2 \rangle_{\nu_c, n_c} \gtrsim d_c. \quad (31)$$

This state is dominated by the adiabatic component in the lowest potential which means that  $\nu_c = 0$ . On the other hand, the states of lowest energy with  $\nu = 0$  might have

an average particle distance less than  $d_c$ . Which number of these excited states is sufficiently large depends on the number of particles and on the scattering length. The ideal condensate is then characterized by one dominating component, i.e.,  $\nu = 0$  and  $|c_{nc}| \simeq 1$  and  $|c_{n \neq nc}| \ll 1$ . If it is impossible to distinguish states with these features it probably makes little sense still to define a condensate. The possible states would be too unstable.

If  $d_c$  is significantly smaller than  $b_t$ , then the state of lowest energy located in the second minimum can be identified as the condensate. This state is characterized by a radial wave function  $f(\rho)$  with the root mean square radius  $\langle \rho^2 \rangle$  approximately equal to the hyperradius at the second minimum of the adiabatic potential  $U_0(\rho)$ .

To be specific we show in fig. 8 the root mean square interparticle distance given by  $\langle r_{ij}^2 \rangle_n = 2\langle \rho^2 \rangle_n / (N-1)$  for the lowest excited states (labeled by  $n$ ) in the potential of fig. 7. All states with  $n \leq 58$  have  $20b \leq \langle r_{ij}^2 \rangle_n^{1/2} \leq 100b$ , which implies that the particles are well outside the range of the interaction with each other. Whether the average distances qualify them as condensates depends on the decay rate of these states. Without barrier these states could extend very far and exhibit Efimov features.

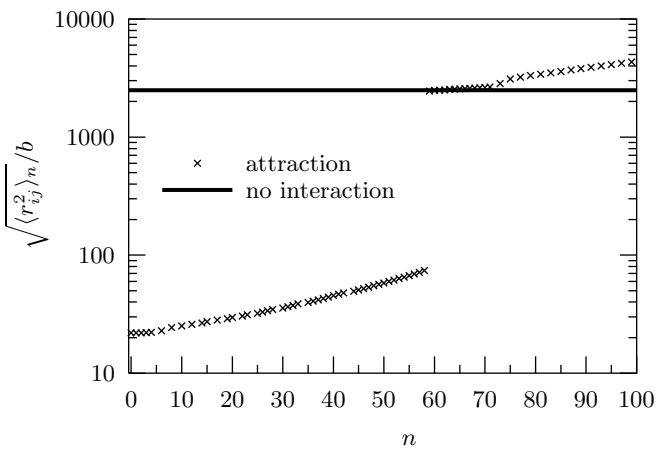


FIG. 8: The root mean square distance for  $\nu = 0$  as a function of the quantum number for  $N = 100$ ,  $a_s/b = -1$ ,  $b_t/b = 1442$ .

For the positive energy states ( $n \geq 59$ ) we encounter a discontinuity in the average particle distance which now exceeds  $2000b$ . In fact we now find  $\langle r_{ij}^2 \rangle \simeq 3b_t^2$  which approximately is obtained in the limit of a non-interacting gas. This investigation could be repeated for the higher adiabatic potentials,  $\nu \geq 1$ , still neglecting the couplings. The same pattern is obtained although there are fewer states with small interparticle distance.

### C. Interaction energy

The total energy of a state in the first minimum only depends on the interaction as these states are self-bound

and stable even without the presence of the external field. These states have no analogue in mean-field calculations. Total energies of the states in the second minimum are dominated by the contribution from the confining field and therefore are rather insensitive to anything else than this field and the corresponding harmonic oscillator quantum numbers. It is then much more informative to compare interaction energies where the large external field contribution is removed.

In fig. 9 is shown the interaction energy per particle as a function of the particle number for a relatively weak attraction corresponding to a small scattering length of  $a_s/b = -0.84$ . The Gross-Pitaevskii solution is stable and the related interaction energy is negative due to the attraction between the particles. A nearly linear behaviour is observed at small particle numbers, since each particle interacts with  $N - 1$  other particles. As  $N$  increases the mean-field attraction increases and the non-physical Thomas collapse is inevitable. This instability occurs for  $N|a_s|/b_t = 0.58$  which corresponds to  $N = 1000$  with the present set of parameters. There is no stable solution to the Gross-Pitaevskii equation for  $N|a_s|/b_t > 0.58$ .

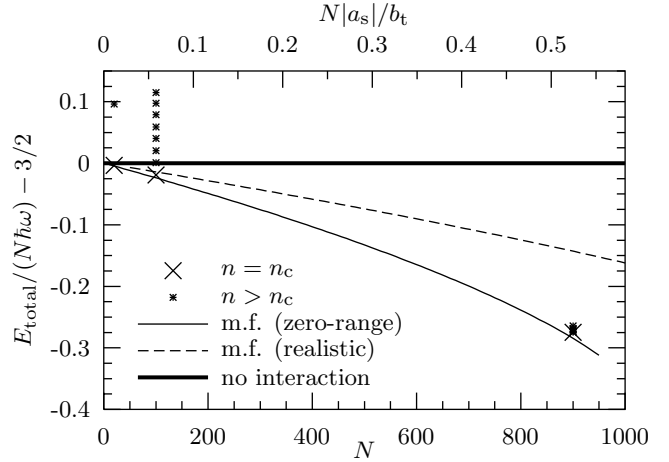


FIG. 9: Gross-Pitaevskii interaction energy (solid curve) as a function of  $N$  for  $a_s/b = -0.84$  and  $b_t/b = 1442$ . Also shown are the hyperspherical calculation for three numbers of particles and  $a_s/b = -0.84$  ( $a_B/b = -0.5$ ) with quantum numbers as indicated [ $n_c = 7$  for  $N = 20$  ( $N|a_s|/b_t = 0.012$ ),  $n_c = 52$  for  $N = 100$  ( $N|a_s|/b_t = 0.058$ ), and  $n_c = 88$  for  $N = 900$  ( $N|a_s|/b_t = 0.52$ )]. The dashed line shows the Gross-Pitaevskii energy for  $a_s/b = -0.5$ .

These mean-field interaction energies are compared to the results obtained with the correlated wave functions from the present formulation. Now only a few of the large number of bound states for each  $N$ -value resemble the Gross-Pitaevskii solutions with a radius corresponding to the second minimum. For  $N = 20$  the first of these is build on the lowest adiabatic potential with quantum number  $n = 7$  and an interaction energy very close to the Gross-Pitaevskii result, while the next state with  $n = 8$  has a positive interaction energy. This feature is repeated

for increasing  $N$ , i.e., the lowest state characteristic for a condensate is similar to the mean-field result and the higher-lying states in the second minimum has smaller interaction. When the Thomas collapse sets in the correlated solutions are still stable due to the use of the finite-range potential.

The correlated and mean-field interaction energies are remarkably similar when both exist. It may at first appear odd that the mean-field interaction energy is marginally lower than by use of the better suited form of the correlated wave function. The reason is that we compare the mean-field result for an effective interaction which has the correct scattering length in the Born approximation while the correlated solution is obtained for an interaction with the correct scattering length. The mean-field interaction is effectively more attractive. The more reasonable comparison is to use an interaction with the same scattering length in both calculations.

The proper comparison is then a Gross-Pitaevskii calculation with  $a_s/b = -0.5$ , corresponding to the Born approximation for a Gaussian of  $a_B/b = -0.5$  with true scattering length  $a_s/b = -0.84$ . As seen in fig. 9 (dashed curve) now the mean-field interaction energies are much smaller. It is remarkable that the correlated solution essentially reproduces the energy of the mean-field calculation where the interaction is renormalized to reproduce the correct energy with the wrong wave function. The large-distance average properties of weakly interacting systems are at best obtained in mean-field computations. All features of correlations are absent by definition.

## V. DECAY RATES

The radial potentials are sensitively depending on the scattering length. In fig. 10 we illustrate the different behaviour by using the angular eigenvalues parametrized through eqs. (20), (21), (26), and (27). In fig. 10a the scattering length is relatively small and a large barrier separates the outer minimum from the inner region. By increasing the scattering length the barrier decreases first into a relatively flat region as in fig. 10b and then disappears completely as in fig. 10c when the trap length is exceeded.

The condensate state is unstable due to the neglected couplings into other degrees of freedom. Two different processes can be identified, each associated with a characteristic time scale. The first is formation of bound state dimers by a three-body process where the third particle ensures conservation of energy and momentum. The number of these three-body recombination (rec) events per unit volume and time can be estimated by the upper limit given in [9, 11]:

$$\nu_{\text{rec}} = 67.9 \frac{\hbar |a_s|^4 n^3}{m}, \quad (32)$$

where  $n$  is the density of the gas. This expression can be converted into an estimate of the recombination rate

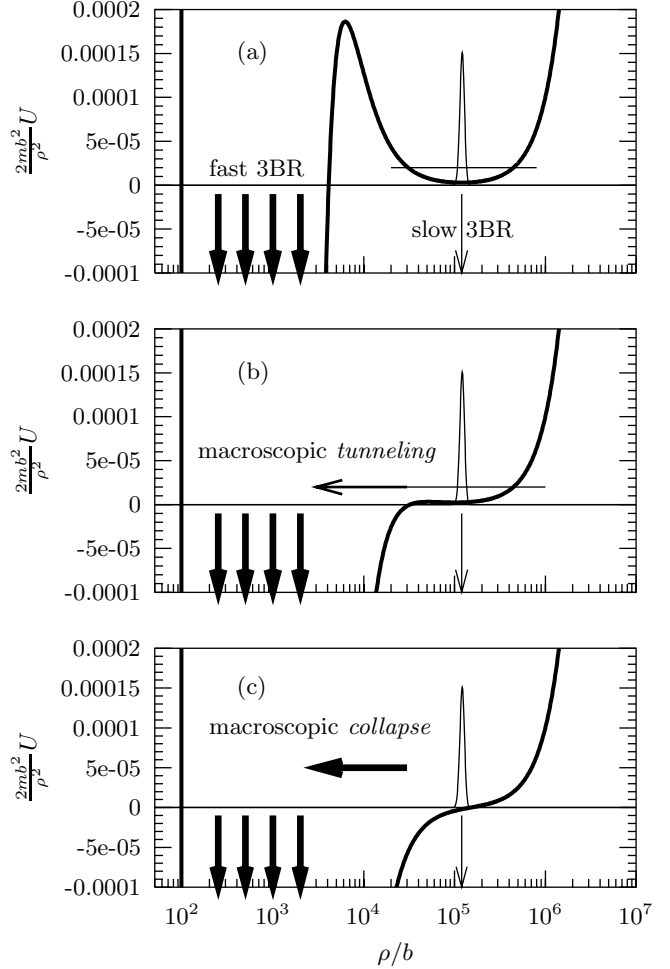


FIG. 10: The radial potential from the schematic model for  $N = 100$ ,  $b_t/b = 10^4$  and a)  $a_s/b = -6$ , b)  $a_s/b = -50$ , c)  $a_s/b \rightarrow -\infty$ . The shown wave function is the lowest radial solution in the non-interacting case. The horizontal lines in parts a) and b) indicate an energy level (not to scale).

for a given hyperradius  $\rho$ . With the volume  $\mathcal{V} = N/n$ , the relation between density and mean distance  $1/n = 4\pi \langle r_{ij}^2 \rangle^{3/2} / 3$ , and  $\langle r_{ij}^2 \rangle = 2\langle \rho^2 \rangle / (N-1)$  obtained from eq. (1), the total recombination rate is

$$\Gamma_{\text{rec}} = \nu_{\text{rec}} \mathcal{V} \simeq 0.5 \frac{\hbar |a_s|^4 N^4}{m \rho^6}, \quad (33)$$

where the mean square average of  $\rho$  is substituted by the coordinate itself. This is entirely in the spirit of the adiabatic hyperspherical expansion method where  $\rho$  is used as a classical parameter. The recombination rate increases rapidly with decreasing  $\rho$ , as indicated by the vertical arrows in fig. 10.

The second decay process is related to macroscopic tunneling through the barrier, as indicated in fig. 10b. The model provides stationary eigenstates which by definition are time independent. Thus, strictly the states do not tunnel through the barrier, but an exponentially

small tail extends to small hyperradii. All particles would immediately recombine into molecular clusters, because the density is very large in the inner region. The rate of this two-step decay, i.e., tunneling through the barrier and subsequent recombination, can be computed as the knocking rate multiplied by the transmission coefficient, which is a measure of the ratio of the probabilities at the turning points inside and outside the barrier. The rate of recombination due to macroscopic tunneling can then be estimated semi-classically by [22]

$$\frac{\Gamma_{\text{tunnel}}}{\hbar} \simeq \frac{N\nu}{1 + e^{2\sigma}}, \quad (34)$$

$$\nu = \frac{1}{2\pi} \sqrt{\frac{1}{m} \frac{d^2 U(\rho)}{d\rho^2}} \bigg|_{\rho_{\text{min}}}, \quad (35)$$

$$\sigma = \int_{\rho_{\text{in}}}^{\rho_{\text{out}}} d\rho \sqrt{\frac{2m}{\hbar^2} [U(\rho) - E]}, \quad (36)$$

where the factor  $N$  is needed to give the total number of recombined particles. Here  $\rho_{\text{min}}$  is the position of the second minimum of  $U$  and  $\rho_{\text{in}}$  and  $\rho_{\text{out}}$  are the classical turning points of the barrier.

The barrier depends strongly on the combination  $N|a_s|/b_t$  [22, 26]. When  $N|a_s|/b_t \ll 1$  the barrier is large and the very small rate can be estimated through eqs. (34), (35), and (36). The WKB action integral is

$$\sigma \simeq \frac{3}{2} N \ln \left( \frac{b_t}{N|a_s|} \right). \quad (37)$$

The barrier is absent when  $N|a_s|/b_t \geq 0.53$ . Close to, but before reaching, this threshold of stability we find the WKB-exponent to be

$$\sigma \simeq 1.7N\delta_s, \quad \delta_s \equiv 1 - \frac{N|a_s|/b_t}{0.53}, \quad (38)$$

which is valid when  $\delta_s$  is close to zero.

Defining the recombination time scale  $T_{\text{rec}}$  by  $N(t) = N(0) \exp(-t/T_{\text{rec}})$  we obtain  $\Gamma_{\text{rec}}/\hbar = -dN/dt = N/T_{\text{rec}}$ , so

$$T_{\text{rec}} = \frac{N\hbar}{\Gamma_{\text{rec}}} = \frac{2m\rho^6}{\hbar|a_s|^4 N^3} = \frac{m\bar{r}_{ij}^6}{4\hbar|a_s|^4}, \quad (39)$$

where we used  $\bar{r}_{ij} = \sqrt{2/N}\rho$ . The final expression is independent of  $N$ . Since the condensate has to form in the external trap it is reasonable to demand that the system is stable versus recombination events on a time scale,  $T_c$ , which is given by the oscillator time scale multiplied by a number  $M$ , i.e.,  $T_{\text{rec}} > T_c \equiv M2\pi/\omega$ . With  $1/\omega = mb_t^2/\hbar$  we get that the condensate is stable when  $\bar{r}_{ij} > \sqrt[6]{8\pi M}|a_s|^{2/3}b_t^{1/3} = d_c$ , where we now obtained an expression for  $d_c$  introduced in section IV B. In units of  $b_t$  we have

$$\frac{d_c}{b_t} = \sqrt[6]{8\pi M} \left( \frac{|a_s|}{b_t} \right)^{2/3}, \quad (40)$$

where the main parameter is  $(|a_s|/b_t)^{2/3}$ .

Thus for  $|a_s|/b_t \lesssim 1$  also  $d_c/b_t \lesssim 1$ . The average particle distance  $\bar{r}_{ij}$  for a state located in the second minimum is of the order  $b_t$  and therefore  $\bar{r}_{ij} \gtrsim d_c$ , i.e., for these states  $\bar{r}_{ij}$  is larger than the critical stability length  $d_c$ . These states then qualify as condensates. For  $^{87}\text{Rb}$  atoms ( $a_s \simeq 100$  a.u.) trapped in a field of  $\nu \simeq 100$  Hz we obtain  $T_{\text{rec}} \sim 7$  days

The barrier vanishes when  $N|a_s|/b_t \simeq 0.53$  [12, 13], which due to the factor of  $N$  implies that  $|a_s|/b_t \ll 1$ . Therefore close to this threshold  $\bar{r}_{ij} \sim b_t \gg d_c$ , i.e., the three-body recombination does not limit the stability of a condensate. In the limit  $\sigma \ll 1$  we get explicitly

$$\frac{\Gamma_{\text{rec}}}{\Gamma_{\text{tunnel}}} \simeq \frac{1}{7.0N^4} \ll 1 \quad (41)$$

implying that the macroscopic tunneling process dominates. With  $\sigma \ll 1$  we obtain that  $\Gamma_{\text{tunnel}}/\hbar \simeq 0.5N\nu$ , which yields a tunneling time of about  $1/\nu$ . For the case with  $\nu \simeq 100$  Hz we therefore obtain a macroscopic tunneling time scale of 10 ms. This is much faster than the three-body recombination time scale, which close to stability is given by

$$\frac{T_{\text{rec}}}{T_{\text{tunnel}}} = \frac{\Gamma_{\text{tunnel}}}{\Gamma_{\text{rec}}} \simeq 7.0N^4 \gg 1. \quad (42)$$

The three-body recombination rate is in fig. 11 shown as a function of hyperradius (solid curve) and compared with the macroscopic tunneling rate (dashed curve) where all particles in the condensate simultaneously disappear. At small hyperradii the three-body recombination rate is clearly much larger than the macroscopic tunneling rate, whereas the opposite holds for large hyperradii. For the chosen set of parameters we find that the two time-scales are roughly equal around the second minimum where the condensate is located. However, the tunneling rate depends strongly on the barrier through the combination  $N|a_s|/b_t$ .

Varying either of the three quantities would then move the tunneling rate up or down in fig. 11. For a larger barrier the condensate would only decay by direct recombination. For a smaller barrier macroscopic tunneling would dominate and the condensate would collapse by “collective” recombination of all particles in a very short time interval.

When a few particles recombine into dimers and leave the condensate, the remaining system is no longer in an eigenstate of the corresponding new hamiltonian. An adiabatic adjustment of hamiltonian and wave function could then take place. Since fewer particles and unchanged  $a_s$  and  $b_t$  means a larger barrier, the stability against macroscopic collapse of the new system is therefore increased.

This stabilization by particle “emission” could also be the result of the recombination in the macroscopic tunneling process if the time-scale for recombination at the relevant small distances is longer than the adiabatic adjustment time. In a possible development first a number

of particles are emitted, the adjustments follow, and a larger barrier appears which traps and stabilizes the part of the initial wave function in the second minimum. However, now fewer particles make out the condensate.

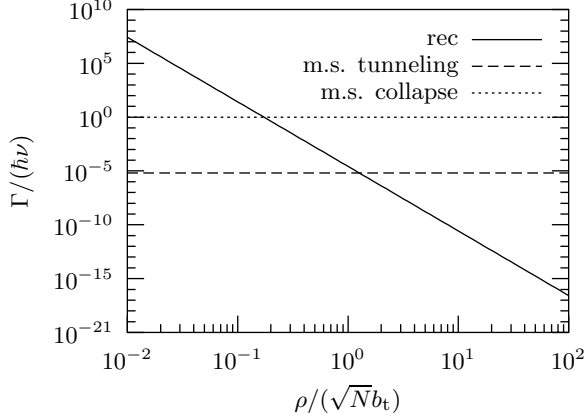


FIG. 11: Three-body recombination rate eq. (33) in units of the oscillator frequency  $\nu = \omega/(2\pi)$ , typically of the order of 10-100 Hz [13], as a function of hyperradius for  $N = 100$ ,  $a_s/b = -50$ ,  $b_t/b = 10^4$ . Shown as the horizontal, dashed line is the macroscopic tunneling rate eq. (34). Shown as the horizontal, dotted line is the macroscopic collapse rate eq. (43) when the scattering length is much larger than the trap length.

These scenarios are open for direct experimental investigations since the interaction can be changed in an experiment by using the Zeeman splitting to tune to a Feshbach resonance [12, 13, 38]. An initial value of the scattering length (corresponding to a stable condensate in the second minimum) can almost instantaneously be changed to a value where the barrier is removed. The initial wave function for the condensate is now no longer a stationary state in the new potential.

If we assume that the only excitations are the degrees of freedom contained in the lowest new hyperspherical potential with s-waves, we can use the sudden approximation and expand on the corresponding eigenfunctions. The most important levels are then the lowest-lying positive energy states with energies comparable to the initial condensate. The time-scale for the time evolution of the initial state in the new potential is then determined by the energy differences between such levels. These states of positive energy and large spatial extension confined by the trap are roughly separated by the oscillator quantum of energy  $\hbar\omega$ . The corresponding rate for populating smaller distances with the consequence of immediate recombination is then crudely estimated to be

$$\frac{\Gamma_{\text{collapse}}}{\hbar} \sim \frac{1}{T} \sim \frac{\omega}{2\pi}. \quad (43)$$

Experimentally [13] the macroscopic collapse time is verified to be of the order  $\sim 1/\omega$ , typically a few milliseconds, as given by the external trapping field.

This macroscopic collapse time is shorter than the macroscopic tunneling time for the parameters of the system in fig. 11. The motion in the potential is fast or slow compared to the recombination time for distances in the first or second minimum, respectively. The time evolution after the sudden removal of the barrier could then be a macroscopic collapse towards smaller hyperradii where dimers and trimers are “emitted” and the barrier begins to appear. The part of the wave function trapped at large distances in the second minimum can then stabilize into a condensate with fewer particles. The time-scale for these processes should then be between the macroscopic collapse time and the recombination time at the second minimum. Possibly other time scales due to the neglected degrees of freedom (angular momentum, clusterization, etc.) could be present in the full study of the dynamics of a many-boson system.

## VI. CONCLUSION

Correlations in a system of  $N$  identical bosons of low density are described by use of a hyperspherical adiabatic expansion. The wave function is decomposed in additive Faddeev-Yakubovskii components, where each term is related to one pair of particles and only s-waves are included. The adiabatic potentials are only weakly coupled and we investigate structures where only the lowest contributes. We use a finite-range attractive or repulsive Gaussian interaction and extract general properties of the lowest angular eigenvalue. We establish universal scaling relations for arbitrary scattering length and particle number. Only the short-distance behaviour is influenced by the choice of interaction potential.

The large-distance asymptotic behaviour is found numerically to reproduce the mean-field result for a zero-range interaction renormalized to give the correct scattering length in the Born approximation. This is remarkable since the correct scattering length for the Gaussian potential is far from the Born approximation. Thus the different terms in the second-order integro-differential equation conspire to produce this large-distance result, which is rigorously established for three particles and on general grounds also expected for many particles.

The intermediate distances outside the range of the interaction also follow universal scaling rules. We parametrize the model-independent part of the effective radial potential in a simple form with an interaction part, a centrifugal barrier term and a contribution from the external field. This potential diverges at small distances due to the centrifugal barrier and at large distances due to the confining external field. The two minima are generally separated by a barrier. The deepest minimum at small to intermediate distances supports self-bound  $N$ -body systems where the density is much larger than for a Bose-Einstein condensate. The second minimum at a much larger distance allows solutions with properties characteristic of a condensate. We distinguish, when pos-

sible, by formulating a definition of a condensate in this context. We compare properties of the correlated structures with those of the zero-range mean-field solutions.

The stability of the condensate is limited by decay into lower-lying many-body cluster states reached by processes where three-body recombination resulting in bound dimers is very prominent. We compute various rates of decay and discuss the time-scales involved. The bare three-body recombination process is strongly density dependent and therefore increases dramatically when the wave packet moves from the second minimum to smaller distances. An intermediate barrier would only allow quantum tunneling followed by a macroscopic collapse. When this barrier is very small by choice of parameters the macroscopic tunneling rate would dominate. When the interaction is changed during an experiment and the barrier is totally removed the already created condensate would collapse and a number of cluster configurations would appear. Stability may be restored and a new condensate created with fewer particles.

In conclusion, we have discussed properties of condensates and extracted universal scaling relations. We have focused on the effects of correlations for large scattering lengths where the mean-field approximation breaks down. Finally we investigated time-scales for various decay mechanisms limiting the stability of the condensate.

## APPENDIX A: NUMERICAL DETAILS

The angular equation can be scaled by using the potential range  $b$  as the unit length [27]. The only interaction parameter is then the Born approximation to the scattering length in this unit  $a_B/b$ . The only length coordinate is measured by  $\rho/b$ . All physical quantities are functions of such dimensionless ratios.

The s-wave two-body scattering length is the node of the zero-energy solution to the two-body Schrödinger-equation, i.e.,  $u(r) \propto (r - a_s)$ . Table II shows the scattering length  $a_s$  for different potential strengths  $a_B$ . The Born-approximation equals the correct scattering length only in the limit of weak attraction, where the scattering length  $a_s$  is much smaller than the range of the interaction  $b$ .

To exemplify, in experimental work  $^{87}\text{Rb}$  atoms with a scattering length of  $a_s = 100$  a.u. are trapped in an external trap of frequency  $\nu = 100$  Hz [22]. Assuming an interaction range around  $b = 1$  nm we obtain  $a_s/b = 5.29$ ,  $b_t/b = 1442$ . This can be modelled by a Gaussian two-body interaction with  $a_B/b = -1.5$ , where the lowest solution corresponds to two-body bound states and the next accounts for the properties of the condensate.

## APPENDIX B: DERIVATIONS

The angular eigenvalue for large scattering length  $a_s$  is independent of hyperradius  $\rho$  when  $\rho$  is large compared

TABLE II: The scattering length  $a_s$  in units of  $b$  for various strengths of a Gaussian potential measured as  $a_B/b$ . The number  $N_B$  indicates the number of bound two-body states.

$a_B/b$	$a_s/b$	$N_B$
+3.625	+1.00	0
-0.35600	-0.50	0
-0.50000	-0.84	0
-0.551	-1.00	0
-1.00000	-5.98	0
-1.069	-10.0	0
-1.18600	-401	0
-1.18765	-799	0
-1.18900	-4212	0
-1.20280	+100	1
-1.33800	+10.0	1
-1.500	+5.29	1
-6.868	-1.00	1
-7.6612	-10.0	1

to the range  $b$  of the potential but small compared to  $a_s$ . The plateau value  $\lambda_\infty$  can be estimated by considering the approximate two-body binding energy

$$E^{(2)} \simeq -\frac{\hbar^2}{ma_s^2}. \quad (\text{B1})$$

In the case where a two-body bound state is present, the highest-lying many-body Efimov-like state has energy approximately equal to this two-body energy. This energy can also be determined as the classical turning point  $\rho_a$  in the radial potential, which coincides with the end of the constant level in the angular eigenvalue:

$$E^{(2)} \simeq U(\rho_a) = \frac{\hbar^2}{2m\rho_a^2} \left( \frac{9N^2}{4} + \lambda_\infty \right). \quad (\text{B2})$$

Combining eqs. (B1) and (B2) and rearranging yields

$$\lambda_\infty(N) \simeq -\frac{2\rho_a^2}{a_s^2} - \frac{9N^2}{4}. \quad (\text{B3})$$

The plateau ends when it intersects with  $\lambda_\delta$ , eq. (18)

$$\lambda_\infty(N) = \lambda_\delta(N, \rho_a) \simeq \frac{3}{2} \sqrt{\frac{3}{\pi}} N^{7/2} \frac{a_s}{\rho_a}. \quad (\text{B4})$$

Combining eqs. (B3) and (B4) yields for large  $N$

$$\rho_a \simeq \sqrt[3]{\frac{3}{4}} N^{7/6} |a_s|, \quad (\text{B5})$$

$$\lambda_\infty(N) \simeq -\sqrt[3]{\frac{9}{2}} N^{7/3} \simeq -1.65 N^{7/3}, \quad (\text{B6})$$

which is very close to the numerical results in eqs. (19) and (29).

---

[1] S. N. Bose, Z. Phys. **26**, 178 (1924).

[2] M. H. Anderson *et al.*, Science **269**, 198 (1995).

[3] C. C. Bradley, C. A. Sackett, J. J. Tollett, and R. G. Hulet, Phys. Rev. Lett. **75**, 1687 (1995).

[4] K. B. Davis *et al.*, Phys. Rev. Lett. **75**, 3969 (1995).

[5] M. Edwards and K. Burnett, Phys. Rev. A **51**, 1382 (1995).

[6] G. Baym and C. J. Pethick, Phys. Rev. Lett. **76**, 6 (1996).

[7] F. Dalfovo, S. Giorgini, L. P. Pitaevskii, and S. Stringari, Rev. Mod. Phys. **71**, 463 (1999).

[8] C. J. Pethick and H. Smith, *Bose-Einstein Condensation in Dilute Gases* (Cambridge University Press, Cambridge, 2001).

[9] E. Nielsen and J. H. Macek, Phys. Rev. Lett. **83**, 1566 (1999).

[10] B. D. Esry, C. H. Greene, and J. P. Burke, Jr, Phys. Rev. Lett. **83**, 1751 (1999).

[11] P. F. Bedaque, E. Braaten, and H.-W. Hammer, Phys. Rev. Lett. **85**, 908 (2000).

[12] J. L. Roberts *et al.*, Phys. Rev. Lett. **86**, 4211 (2001).

[13] E. A. Donley *et al.*, Nature (London) **412**, 295 (2001).

[14] S. K. Adhikari, Phys. Rev. A **66**, 013611 (2002).

[15] S. K. Adhikari and P. Muruganandam, J. Phys. B **35**, 2831 (2002).

[16] R. Jastrow, Phys. Rev. **98**, 1479 (1955).

[17] S. Cowell *et al.*, Phys. Rev. Lett. **88**, 210403 (2002).

[18] C. C. Moustakidis and S. E. Massen, Phys. Rev. A **65**, 063613 (2001).

[19] L. D. Faddeev, J. Exptl. Theoret. Phys. (U.S.S.R.) **39**, 1459 (1960) [Sov. Phys. JETP **12**, 1014 (1961)].

[20] O. A. Yakubovskii, Yad. Fiz. **5**, 1312 (1967) [Sov. J. Nucl. Phys. **5**, 937 (1967)].

[21] B. D. Esry and C. H. Greene, Phys. Rev. A **60**, 1451 (1999).

[22] J. L. Bohn, B. D. Esry, and C. H. Greene, Phys. Rev. A **58**, 584 (1998).

[23] N. Barnea, Phys. Lett. B **446**, 185 (1999).

[24] D. Blume and C. H. Greene, Phys. Rev. A **66**, 013601 (2002).

[25] S. Jonsell, H. Heiselberg, and C. J. Pethick, Phys. Rev. Lett. **89**, 250401 (2002).

[26] O. Sørensen, D. V. Fedorov, and A. S. Jensen, Phys. Rev. Lett. **89**, 73002 (2002).

[27] O. Sørensen, D. V. Fedorov, and A. S. Jensen, Phys. Rev. A **66**, 032507 (2002).

[28] O. Sørensen, D. V. Fedorov, A. S. Jensen, and E. Nielsen, Phys. Rev. A **65**, 051601 (2002).

[29] A. Bijl, Physica **7**, 869 (1940).

[30] R. B. Dingle, Phil. Mag. **40**, 573 (1949).

[31] D. V. Fedorov and A. S. Jensen, Phys. Rev. Lett. **71**, 4103 (1993).

[32] A. S. Jensen, E. Garrido, and D. V. Fedorov, Few-Body Syst. **22**, 193 (1997).

[33] D. V. Fedorov and A. S. Jensen, Phys. Rev. A **63**, 063608 (2001).

[34] E. Nielsen, D. V. Fedorov, A. S. Jensen, and E. Garrido, Phys. Rep. **347**, 373 (2001).

[35] A. Bulgac, Phys. Rev. Lett. **89**, 050402 (2002).

[36] V. Efimov, Phys. Lett. **33B**, 563 (1970).

[37] U. V. Poulsen, Ph.D. thesis, Department of Physics and Astronomy, University of Århus, Denmark, 2002.

[38] S. Inouye *et al.*, Nature (London) **392**, 151 (1998).